OPEN ACCESS
IOP Publishing

Made open access 20 September 2017
Journal of Physics G: Nuclear and Particle Physics

J. Phys. G: Nucl. Part. Phys. **44** (2017) 064002 (21pp) https://doi.org/10.1088/1361-6471/aa6642

Collinear laser spectroscopy at ISOLDE: new methods and highlights

R Neugart[1,2], J Billowes[3], M L Bissell[3], K Blaum[1], B Cheal[4], K T Flanagan[3], G Neyens[5], W Nörtershäuser[6] and D T Yordanov[7]

[1] Max-Plank-Institut für Kernphysik, D-69117 Heidelberg, Germany
[2] Institut für Kernchemie, Universität Mainz, D-55128 Mainz, Germany
[3] School of Physics and Astronomy, The University of Manchester, Manchester, M13 9PL, United Kingdom
[4] Oliver Lodge Laboratory, Oxford Street, University of Liverpool, Liverpool, L69 7ZE, United Kingdom
[5] Instituut voor Kern- en Stralingsfysica, KU Leuven, Celestijnenlaan 200 D, B-3001 Leuven, Belgium
[6] Institut für Kernphysik, TU Darmstadt, D-64289 Darmstadt, Germany
[7] Institut de Physique Nucléaire, CNRS-IN2P3, Université Paris-Sud, Université Paris-Saclay, F-91406 Orsay, France

Received 5 December 2016, revised 27 February 2017
Accepted for publication 13 March 2017
Published 19 April 2017

Abstract

Over three and a half decades of collinear laser spectroscopy and the COLLAPS setup have played a major role in the ISOLDE physics programme. Based on a general experimental principle and diverse approaches towards higher sensitivity, it has provided unique access to basic nuclear properties such as spins, magnetic moments and electric quadrupole moments as well as isotopic variations of nuclear mean square charge radii. While previous methods of outstanding sensitivity were restricted to selected chemical elements with special atomic properties or nuclear decay modes, recent developments have yielded a breakthrough in sensitivity for nuclides in wide mass ranges. These developments include the use of bunched beams from the radiofrequency quadrupole cooler–buncher ISCOOL, which allows a suppression of background by several orders of magnitude. Very recently, the combination of collinear laser spectroscopy with the principle of laser resonance ionisation took shape in the new CRIS setup, providing a very selective and efficient detection of optical resonance. We outline the basic experimental developments and discuss important results on nuclei or chains of isotopes in different mass ranges.

Keywords: nuclear moments and radii, laser spectroscopy, exotic isotopes

1. Introduction

Collinear laser spectroscopy has been introduced at ISOLDE for the investigation of fundamental properties of exotic nuclei such as nuclear ground state spins, electromagnetic moments and charge radii. These quantities are obtained from high-resolution measurements of atomic spectral lines which exhibit hyperfine structure and isotope shift caused by the interaction of the shell electrons with the nucleus [1]. Depending on the atomic properties and the availability of suitable laser wavelengths, these experiments can be performed on the singly-charged ions delivered by ISOLDE or on neutral atoms obtained by charge exchange when the beam passes through an alkali vapour cell.

The tradition of collinear laser spectroscopy at ISOLDE goes back to 1980, when the first COLLAPS setup was completed and first successful experiments were performed on the neutron-rich barium isotopes [2, 3]. Numerous studies of further isotopic chains mainly in the heavier-mass region followed during the first 10 years of operation, up to the end of ISOLDE-2 in 1990. A second period of COLLAPS operation, starting with the commissioning of PSB–ISOLDE, concentrated on the study of lighter nuclear systems and was combined with a diversification of experimental techniques. The work of this period was the main subject of the previous report, published in the ISOLDE Laboratory Portrait of 1999 [4].

The efforts in that period were focussed on the development of highly sensitive experimental techniques, exploiting the properties of special classes of atomic systems. Standard collinear spectroscopy is based on a single resonant excitation and the fluorescence decay from the excited level is used as a straightforward detection method. However, optical fluorescence detection is rather inefficient and suffers from background photons due to the scattered laser light. The signal-to-noise ratio limits such experiments to isotopes produced at rates of typically more than 10^6 ions s^{-1}. Studies of more exotic (less produced) isotopes became possible in the 1990s by a variety of particle- or radiation-detection techniques based on laser optical pumping. These schemes provide higher efficiency and less background, which considerably enhances the sensitivity. Beams with rates down to 10^3 ions s^{-1}, in favourable cases even somewhat below 100 ions s^{-1} [5], are usually sufficient for an experiment.

These particle/radiation detection techniques require each a dedicated experimental setup at the collinear beam line, and each technique is only applicable on particular elements or isotopes. For example, optical pumping of neutral atoms, detected by state-selective collisional ionisation [6] and optical pumping of singly-charged ions, detected by state-selective neutralisation [7, 8] are suitable techniques for the noble gasses (e.g. Ar isotopes) and alkaline earth elements (e.g. Ca and Sr isotopes), respectively. Beta-asymmetry detection after optical pumping with circularly polarised laser light is applicable to isotopes with short half-lives (less than a few seconds), primarily to alkali-like systems [9, 10], but is less element-specific. The latter method has been used in the past decade very successfully to study the deformation of the ^{11}Li halo nucleus [11] and the changing nuclear structure of the Mg isotopes towards and in the 'island of inversion' [12], as discussed in more detail in section 3.1.

Very recently, a particular solution to the problem of sensitive and background-free particle detection was chosen for the CRIS setup (section 3.3). Instead of using a single narrow-band laser beam and state-selective secondary processes for the detection of optical pumping, the collinear resonance ionisation method uses a second (or third) laser to further excite the level populated in the first high-resolution step to the continuum and thus ionise the atoms. This is a very selective process which allows the detection of optical resonance by counting ions very efficiently and virtually without any background.

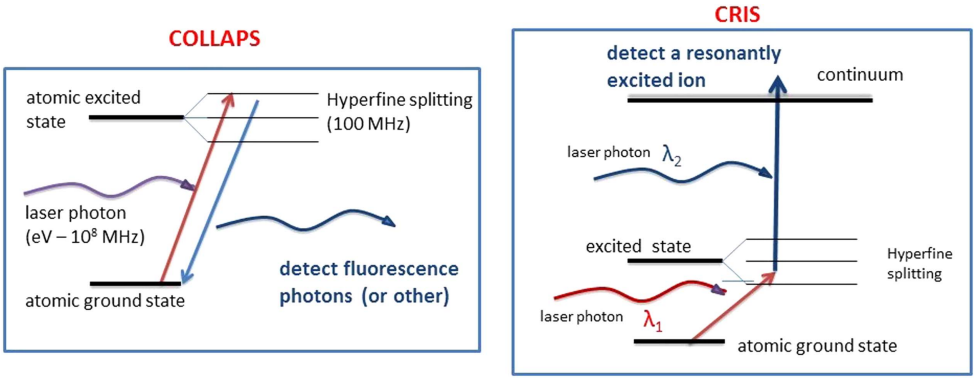

Figure 1. Schematic representation of two laser spectroscopy experiments at ISOLDE and their specifications. Left: the scheme used at the COLLAPS beam line with a variety of detection techniques. Right: a scheme for a typical collinear resonance ionisation spectroscopy experiment at CRIS.

Nowadays two types of collinear laser spectroscopy experiments can be distinguished: collinear laser spectroscopy using one single continuous wave (cw) laser for the resonant excitation of an ionic (or atomic) hyperfine structure (figure 1, left panel) or collinear resonance ionisation spectroscopy (CRIS) using a second (or third) laser to subsequently ionise the resonantly excited atom (figure 1, right panel).

An important breakthrough in the sensitivity of classical collinear laser spectroscopy has been achieved with the installation of the ion cooler–buncher ISCOOL [13] in the form of a gas-filled radiofrequency quadrupole (RFQ) trap at the HRS mass separator. By bunching the ion beam, and by recording only the resonance fluorescence signal during the time the ion bunch appears in front of the photomultiplier tubes, the background in the photon detection is reduced by factors up to 10 000, implying a gain in sensitivity by about two orders of magnitude. Since the fall of 2008, nearly all optical detection experiments at COLLAPS have been performed using this new method on bunched beams from ISCOOL. They mainly cover the medium-mass region between $Z \approx 20$ and $Z \approx 50$ as discussed in section 3.2.

Bunching of the beam also offers decisive advantages for the CRIS experiments using resonance ionisation. The bunches from ISCOOL are synchronised with the pulsed ionisation lasers, which means that all atoms delivered from ISOLDE can interact with the light and the full duty cycle is available for excitation and subsequent ionisation. The detection of ions is very efficient and quasi background-free, since ultra-high vacuum (UHV) in the interaction region highly reduces the background which originates from collisional ionisation of isobaric beam contaminants. The stepwise resonance ionisation scheme (using pulsed lasers) is also used for low-resolution in-source laser spectroscopy experiments [14], where high efficiency and selectivity allow experiments on beams with rates of less than 1 ion s^{-1} and in some cases even 0.01 ions s^{-1} [15]. Details of the CRIS technique and first promising results obtained since 2012 will be discussed in section 3.3.

2. Experimental principle of collinear laser spectroscopy

Hyperfine splittings of the order of 10–1000 MHz and ionic (atomic) transitions in the visible frequency range ($\sim 10^{15}$ Hz) require very high spectroscopic resolution, better than 10^{-7}–10^{-8}. A particular challenge is the spectroscopy of light elements, because both the hyperfine

interaction of nuclear moments with the shell electrons and the influence of the nuclear volume on the atomic energy levels (field shift) scale roughly with Z^2.

The hyperfine structure is usually dominated by the magnetic interaction between the nucleus and the shell electrons, which gives access to the magnetic moments of nuclei. Nuclear spins are directly obtained from the relative hyperfine structure intervals provided the electron angular momentum is greater than 1. The interaction of the nuclear quadrupole moment with the electric field gradient produced by the electrons is usually smaller. With the small quadrupole moments of light nuclei it tends to fall below the natural linewidth limit which is of the order of 10 MHz for sufficiently strong optical transitions. Isotope shifts provide information about the changes of nuclear mean square charge radii along a chain of isotopes. For the evaluation of absolute radii these can be combined with radii data which are available for the stable isotopes [16].

The conditions of high resolution and efficient excitation can be fulfilled by applying the collinear laser spectroscopy technique to beams from ISOLDE. In fact, the concept of collinear laser spectroscopy [17] emerged from discussions about a method to be used with radioactive beams. Isotope-separated beams are merged with a narrow-band cw laser beam and resonance excitation is detected by counting the fluorescence photons. The collinear (or anti-collinear) overlap of both beams naturally provides a narrow Doppler width as a consequence of the electrostatic extraction and acceleration from the ion source. All ions in the beam gain the same amount of kinetic energy, which conserves the energy spread. With the kinetic energy being proportional to the square of the velocity this compresses the velocity distribution. A typical energy spread of a few eV on a beam energy of about 40 keV gives a Doppler width of less than 30 MHz, close to the natural linewidth for many atomic/ionic transitions. The Doppler shift can be used to tune the rest frame laser frequency across a resonance structure by slightly changing the velocity of the ions. A high-resolution spectrum is thus recorded by detecting fluorescence photons as a function of a post-acceleration/deceleration voltage applied to the detection chamber. Compared to collinear laser spectroscopy, the in-source laser spectroscopy experiments have to deal with a Doppler broadening in the GHz range, which is typical for the thermal conditions in the ion source [18].

The requirement of high sensitivity calls for efficient excitation which is fulfilled with the Doppler width matching the natural linewidth, which means that optical resonance occurs simultaneously for all ions in the beam. Sensitivity is finally limited by the efficiency of fluorescence photon detection in the presence of background from scattered laser light. This leads to the sensitivity limit of standard collinear laser spectroscopy mentioned in the Introduction. Background reduction with bunched beams has lowered this limit by about two orders of magnitude as will be further discussed in section 3.2.

Often neutral atoms offer more favourable spectroscopic conditions than the singly-charged ions delivered by ISOLDE. This is due to the fact that for many ions the UV wavelengths of suitable spectral lines cannot easily be reached by tunable narrow-band cw lasers. In these cases beams of neutral atoms are obtained by charge-exchange reactions with alkali atoms in a vapour cell. Such processes usually have high cross-sections and occur without noticeable loss in beam quality. Neutralisation of the beam can also be utilised for populating metastable atomic states from which the excitation is easier than from the ground state or which provide more significant nuclear moment or radii information.

This report deals with a number of techniques that are all based on the principles outlined above. We shall see that these techniques aim at a considerable improvement of sensitivity and to some extent are specific for particular elements or isotopes. The field of laser

spectroscopy on beams of radioactive isotopes has been treated more generally in several recent review articles [18–20].

3. New methods and highlights since 2000

In the past fifteen years, collinear laser spectroscopy has been used to study regions in the nuclear chart along magic proton and/or neutron numbers, and in particular to study a variety of nuclear structure effects appearing as a function of isospin. We present the main technical developments along with highlight results obtained in the light, medium and heavy mass regions. Each technical development is presented with the region where it has been applied first.

3.1. Light nuclei up to $Z \approx 12$

3.1.1. Beta-asymmetry detection of optical resonance and nuclear magnetic resonance (NMR). For some light short-lived isotopes the problem of sensitivity can be addressed by optically polarising the nuclei and detecting the polarisation in the angular distribution of β-decay electrons or positrons, which is asymmetric with respect to the nuclear spin direction. With implantation of the beam into a suitable host crystal lattice this has the further advantage of offering an alternative access to the nuclear moments, which is based on NMR detected by the influence of radiofrequency on the β-decay asymmetry (β-NMR). The magnetic moments of nuclei interact with a static magnetic field, while the quadrupole moments interact with an electric field gradient produced at their lattice site in a non-cubic crystal. The latter is particularly important for light atomic systems where the quadrupole interaction is too small to be resolved in the hyperfine structure of spectral lines.

Polarisation occurs by optical pumping between the m_F states of the coupled atomic system of electronic and nuclear spin. The spins are decoupled in the strong magnetic field before entering the host crystal where the nuclear spin polarisation relaxes within typically a few seconds. Resonant interaction of the atoms with the circularly polarised laser light produces atomic and nuclear spin polarisation. After implantation of the polarised radioactive beam in a suitable crystal, a NMR signal is observed as a change in the β-decay asymmetry.

Optical pumping and β-NMR experiments were initiated already at ISOLDE-2 with the goal of measuring the spin and the magnetic moment of the famous two-neutron halo nucleus ^{11}Li [21]. The result of $I = 3/2$ ruled out strong deformation as a possibility to explain the exceptionally large matter radius obtained from break-up cross-sections [22] in high-energy reactions. Later on, with refined NMR techniques, even the quadrupole moment could be determined by measuring the interaction with the electric field gradient at the Li lattice site in a $LiNbO_3$ crystal [23]. In the comparison of ^{9}Li and ^{11}Li it turned out that the two additional (halo) neutrons have little effect on the quadrupole moment.

^{11}Li *revisited.* Based on these achievements a new effort was made after 2000 towards a considerable improvement of the quadrupole moment measurement on ^{11}Li, with the primary goal of detecting an influence of the halo neutrons on the ^{9}Li core which is responsible for the electrical properties. Compared to the previous approach, a new NMR magnet offered a more homogeneous magnetic field and from a systematic study of implantation crystals it became possible to gain an order of magnitude in resolution by replacing the $LiNbO_3$ ionic crystal by a metallic Zn crystal [24]. The multiple-rf resonance technique employed already previously, uses a set of radio frequencies depending on the quadrupole moment Q as a parameter and requires the exact knowledge of the Larmor frequency which is determined by the magnetic moment. For this purpose a new precise measurement of the g-factor ratio between ^{11}Li and

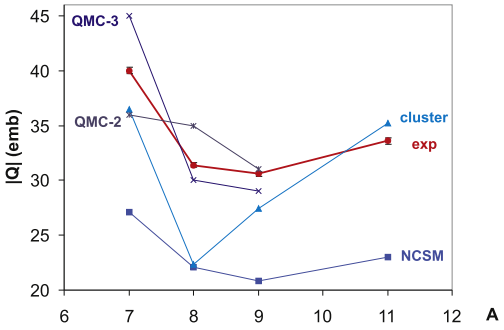

Figure 2. Quadrupole moments of the Li isotopes compared to values from different theoretical models. Reprinted figure with permission from [11], copyright 2008 by the American Physical Society.

^{8}Li was performed in an auxiliary experiment using a cubic Si crystal. The result of $\mu(^{11}\mathrm{Li}) = 3.6712(3)\mu_N$ is an order of magnitude more accurate than the previous value [21], due to the narrow resonance linewidth in the Si crystal as compared to Au or LiF hosts [24].

The quadrupole splitting of the NMR signal of ^{11}Li was measured with reference to ^{9}Li which both have the same spin and similar magnetic and electric moments. In this way systematic uncertainties related to resonance shapes and rf-field broadening could largely be avoided. The result is $Q(^{11}\mathrm{Li})/Q(^{9}\mathrm{Li}) = 1.088(15)$, meaning that the quadrupole moment of ^{11}Li is nearly 10% larger than that of ^{9}Li. We can try to interpret this observation [11] assuming the simple picture of a ^{9}Li core surrounded by two halo neutrons in spherical orbits. From experiment [25, 26] we know that the rms charge radius $\langle r^2\rangle^{1/2}$ increases by 10.2 (2.8)%, from 2.25(5) fm for ^{9}Li to 2.48(4) fm for ^{11}Li, while we find that the quadrupole moment increases by 8.8(1.5)%. For identical deformation of ^{9}Li and ^{11}Li one should expect an increase of the quadrupole moment proportional to the mean square radius $\langle r^2\rangle$. However, if we ascribe the increase of the radius to a recoil effect caused by the spherical halo, the centre-of-mass (CM) movement produces an isotropic expansion of the (non-spherical) charge distribution and the quadrupole moment increases just with $\langle r^2\rangle^{1/2}$. This explains the striking analogy between the quadrupole moments and the rms charge radii without any additional influence of the halo neutrons on the ^{9}Li-core structure.

The trend of experimental quadrupole moments from ^{7}Li to ^{11}Li (figure 2) is perfectly reproduced by a no-core shell model (NCSM) using an effective interaction derived microscopically from a nucleon–nucleon potential fitted to nucleon scattering data [27]. Only the absolute values of all quadrupole moments are about 30% smaller than the experimental values. This may be explained by a limited model space and could be adjusted by using effective charges.

Magnesium. The neutron-rich magnesium isotopes cover the upper sd-shell and range into the so-called island of inversion which is characterised by a disappearance of the $N = 20$ shell gap. For the prominent $N = 20$ nucleus ^{32}Mg strong deformation was postulated from the large $B(\mathrm{E2}; 2^+ \rightarrow 0^+)$ value [28] and this is consistent with the behaviour of other observables as, e.g., the nuclear masses and excitation energies in this region. Measuring nuclear moments and radii of the magnesium isotopes remained a challenge for sensitivity reasons.

At ISOLDE laser ionisation with RILIS offers favourable production conditions for the short-lived odd-*A* isotopes around ^{32}Mg. Optical pumping with sufficient laser power of a few mW can be performed in one of the UV resonance lines of Mg^+ ions at 280 nm and used for

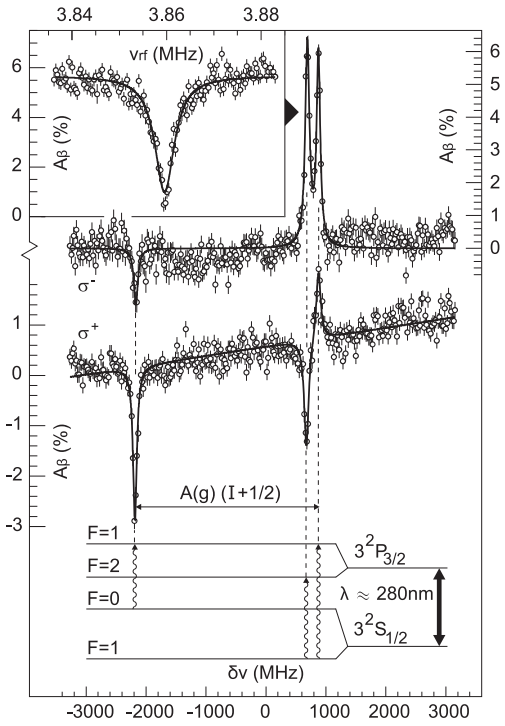

Figure 3. Hyperfine structure (hfs) spectra of σ^+, σ^- optically polarised $^{31}Mg^+$ ions, observed via the asymmetry in the nuclear β-decay after implantation into MgO. The corresponding hfs levels for $I = 1/2$ are shown below. The inset shows an rf magnetic resonance of the implanted nuclei at maximum asymmetry, yielding the nuclear g-factor.

β-NMR experiments. For the longer-lived isotopes closer to stability further interesting information on the radii and moments can be obtained from conventional collinear laser spectroscopy measurements.

The series of experiments covering all these aspects started with a great surprise about the spin and the magnetic moment of ^{31}Mg. This nucleus appeared to be an ideal β-NMR candidate because of the short half-life of 250 ms and a still abundant production of more than 10^5 ions per second. Beta-decay asymmetries up to 10% were reached by excitation in the transition 3s $^2S_{1/2} \rightarrow$ 3p $^2P_{3/2}$ (D2 line). The spin and magnetic moment were measured by combining the results from two experimental techniques, based on the atomic hyperfine structure and on the nuclear interaction with external magnetic fields. With the nuclear g-factor obtained from the NMR Larmor frequency, the spin I was directly deduced from the atomic (ground state) hyperfine structure splitting being proportional to the parameter $g(I + 1/2)$.

Contrary to all expectations from systematics and from shell-model calculations the $N = 19$ nucleus ^{31}Mg turned out to have the spin $I = 1/2$ with a positive parity [29]. This puzzling result initiated some theoretical effort [30] that succeeded to reproduce the level assignments based on the measured ground state spin and confirmed a ground state wave function being dominated by 2p–2h intruder configurations as inferred already from the magnetic moment [29]. Further controversy with conclusions from nuclear spectroscopy and

shell-model theory came up with the measurements on ^{33}Mg yielding $I = 3/2$ combined with a magnetic moment that was consistent only with a negative parity [31, 32]. The ^{33}Mg ground state could again be shown to have a nearly pure 2p–2h intruder nature, contrary to the earlier suggested 1p–1h configuration and in agreement with the structure of other isotopes in the 'island'.

Although the β-decay asymmetry served as a very sensitive method of detecting optical resonance in short-lived isotopes, it remained of limited use for the accurate measurement of isotope shifts. This is a consequence of the complicated line shapes caused by the optical pumping process in a magnetic field varying along the beam path. However, a realistic description of the resonance line shapes is possible if optical pumping is performed in ions for which the interaction with the light can be switched on and off by the Doppler effect and the resonance condition is established only in a well-defined low-magnetic-field region.

The quantitative simulation of the resonance line shapes of a β-asymmetry spectrum is shown in figure 3 for the example of ^{31}Mg. It is the result of optical pumping in a weak magnetic field and subsequent decoupling of the electronic and nuclear spins with detection of nuclear spin polarisation [12]. For measuring the isotope shifts within the chain of magnesium isotopes [33] this feature was exploited for the neutron-rich ^{29}Mg and ^{31}Mg and the neutron-deficient ^{21}Mg. The conventional method of optical resonance detection was used for odd-A isotopes close to stability and on doubly-even isotopes including the special case of ^{32}Mg for which the weak signal had to be brought out from the background by counting photons in coincidence with ions.

The mean square charge radii extracted from these isotope shifts exhibit a minimum around stable ^{26}Mg. This corresponds to a minimum of deformation in the middle of the sd shell around $N = 14$. From the steep increase beyond ^{30}Mg the borderline of the island of inversion is localised between ^{30}Mg and ^{31}Mg, in accordance with the conclusions from spins and magnetic moments.

3.1.2. Collinear–anticollinear spectroscopy on beryllium. Isotope shift measurements on light elements with $Z < 10$ have not been possible at COLLAPS until recently, due to the limitations caused by voltage measurements and the limited knowledge of the exact starting potential of the ions. The acceleration voltage is known to about 10^{-4} relative uncertainty and has even been calibrated to somewhat higher accuracy using a high-precision high-voltage divider [34]. However, this still leads to an uncertainty of about 15 MHz for the isotope shift between ^{9}Be^{+} and ^{11}Be^{+} in the 2s $\rightarrow$ 2p resonance lines, which has to be compared to the expected field-shift contribution of approximately 5 MHz. In order to address this chain of isotopes, a technique that combines collinear laser spectroscopy using counter-propagating and co-propagating laser beams with frequency-comb technology was developed. The beam line setup and the frequency-comb locked laser system are described in detail in [35]. This allowed the measurement of absolute transition frequencies in the laboratory frame for both directions ($\nu_{\pm}$), which are related to the rest-frame frequency ν_0 according to

$$\nu_{\pm} = \nu_0 \gamma (1 \pm \beta). \tag{1}$$

The velocity of the ions $\beta = v/c$ as well as the time dilation factor $\gamma = (1 - \beta^2)^{-1/2}$ depend on the acceleration voltage, but with both absolute transition frequencies measured precisely in the laboratory frame, these variables can be eliminated:

$$\nu_{+} \cdot \nu_{-} = \nu_0^2 \gamma^2 (1 + \beta)(1 - \beta) = \nu_0^2. \tag{2}$$

Hence, the rest-frame transition frequency $\nu_0 = \sqrt{\nu_{+} \cdot \nu_{-}}$ can be extracted without additional knowledge of the ion velocity or acceleration voltage. Spectra taken with co- and counter-

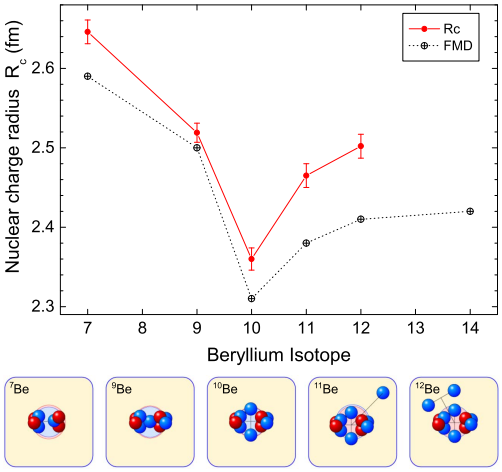

Figure 4. Nuclear charge radii along the beryllium isotopic chain. The red bullets (•) represent the experimental results with error bars dominated by the uncertainty of the reference charge radius of ^{9}Be [39]. Additionally shown are results of fermionic molecular dynamic (FMD) calculations [42], which reproduce the trend along the isotopic chain very well. The bottom row shows a simplified structure of the isotopes interpreted in a cluster picture.

propagating laser beams look like mirror images. This is an additional asset since small inaccuracies from the modelling of the line shape shift the peak centre into opposite directions. Consequently, the respective shift largely cancel each other when taking the geometric average.

Isotope shifts $\delta\nu^{9,A}_{\mathrm{IS,exp}} = \nu^{A} - \nu^{9}$ were measured for $^{7-12}$Be. To extract differences in the mean square nuclear charge radii, these were combined with state-of-the-art *ab initio* atomic structure calculations for the three-electron system [36–38], providing the mass shift $\delta\nu^{A,A'}_{\mathrm{MS,theory}}$ and the field shift factor F with very high accuracy. The radii changes are related to the isotope shifts by

$$\delta\langle r_c^2\rangle^{9,A} = \frac{\delta\nu^{9,A}_{\mathrm{IS,exp}} - \delta\nu^{9,A}_{\mathrm{MS,theory}}}{F}. \tag{3}$$

Total charge radii were then obtained by combining $\delta\langle r_c^2\rangle^{9,A}$ with the known charge radius of the stable isotope ^{9}Be determined using elastic electron scattering [39]. The results, shown in figure 4, reveal a characteristic trend that can be explained by the cluster structure of these light nuclei. This is visualised in a very simplified picture in the small panels below the graph. The lightest isotope ^{7}Be can be regarded as a two-body cluster $\alpha + {}^{3}$He. CM motion blurs the proton distribution and leads to a rather large charge radius. The stable ^{9}Be has an $\alpha + \alpha + n$ structure and is less extended than ^{7}Be due to the compactness of the α particles and the binding strength of the additional neutron. This effect is even enhanced with the second neutron added in ^{10}Be. The sudden upward trend to ^{11}Be is attributed to the one-neutron halo character of ^{11}Be which can be disentangled into a ^{10}Be core and a loosely bound neutron. This halo character increases the matter radius and also affects the charge radius due to the CM motion of the core. The further increase towards ^{12}Be is attributed to a strongly mixed sd character of the two outermost neutrons, indicating the disappearance of the $N = 8$ shell closure for beryllium. A more detailed discussion of the nuclear charge radii in comparison

with *ab initio* microscopic nuclear structure calculations and conclusions about the shell closure can be found in [40–42]. The investigation of both lines of the $2s\ ^2S_{1/2} \rightarrow 2p\ ^2P_{1/2,3/2}$ fine structure doublet also yielded information on the fine-structure splittings for all isotopes [43]. These are in reasonable agreement with advanced calculations by Puchalski and Pachucki [44] and provided an important test of many-body non-relativistic bound-state quantum electrodynamics theory.

3.2. Medium-mass nuclei: from $Z \approx 20$ to $Z \approx 50$

Nearly all experiments discussed in this section have used bunched beams from the ISCOOL ion cooler–buncher [13]. As first demonstrated in experiments at JYFL (Jyväskylä) [45], the bunching can be used for a considerable reduction of the dominating stray-light background of fluorescence-detected collinear laser spectroscopy. Cooling and bunching of the beam is accomplished in a gas-filled linear Paul trap at high voltage in which the ions are captured and released at regular time intervals. The re-accelerated ions arrive at the COLLAPS beam line in bunches of a few microseconds length. This device allows for a time correlation between the resonance fluorescence signal and the ion bunch passing in front of the photomultiplier tubes [46]. With bunches of typically a few μs every 100 ms, the background in the photon detection is considerably reduced and the signal-to-background ratio is improved by a factor of 10 000 compared with a continuous beam, as illustrated in figure 3 of [47]. With the corresponding improvement in sensitivity by a factor of 100, fluorescence-detection-based laser spectroscopy is now routinely possible on beams with rates down to a few 1000 ions s^{-1} and in exceptional cases down to a few 100 ions s^{-1} [48].

The breakthrough achieved by bunched-beam spectroscopy was demonstrated in the experiments on the neutron-rich Cu and Ga isotopes. A spin inversion was observed in the ground state of the odd-mass Cu isotopes, from $I = 3/2$ up to ^{73}Cu, to $I = 5/2$ in ^{75}Cu [49], while the Ga spins and quadrupole moments reveal a change in the shell structure between $N = 40$ and 50 [50]. The latest highlight, achieved on a beam of about 300 ions s^{-1}, was the unexpected increase of the mean square charge radii of the Ca isotopes up to the proposed 'doubly-magic' ^{52}Ca [48]. In this section we will present some general conclusions on physics questions addressed in these experiments. An overview of the experimental results obtained is given in table 1.

3.2.1. Monopole migration of single-particle levels. In the odd-A K ($Z = 20 - 1$) and Cu ($Z = 28 + 1$) isotopes it had been observed that the first-excited-state energy decreases dramatically with an increasing number of neutrons between $N = 20$ and 28 in potassium and beyond $N = 40$ in copper. In the K isotopes the energy of the $1/2^+$ level (due to a hole in the $\pi s_{1/2}$ orbital) decreases gradually as the $\nu f_{7/2}$ level is being filled and this level becomes the ground state in ^{47}K [73]. In the Cu isotopes the $5/2^-$ level energy (due to a proton in the $\pi f_{5/2}$ level) was seen to decrease between ^{69}Cu and ^{73}Cu [74], as the $\nu g_{9/2}$ is being filled.

In 2005 Otsuka *et al* explained this monopole migration of single-particle levels as due to the tensor part of the nucleon–nucleon monopole interaction, and they provided an intuitive explanation as to where and how this monopole migration would occur in the nuclear chart [75]. The interaction is strongest between protons and neutrons, and between nucleons having the same radial quantum number. The interaction is attractive for orbits that have opposite intrinsic and orbital spin, and repulsive between orbits that have their intrinsic and orbital spins in the same direction. The strength of the interaction increases as the orbits are being filled.

Table 1. An overview of measurements made at COLLAPS and CRIS at ISOLDE in the $Z = 20$ to $Z = 50$ region.

Z	Isotopes	Measured	References
K, 19	38, 38m, 39, 42, 44, 46–51	I, μ, $\delta\langle r^2\rangle$	[51–54]
Ca, 20	40, 43–52	I, μ, Q_s, $\delta\langle r^2\rangle$	[48, 55, 56]
Mn, 25	51, 53–64	I, μ, $\delta\langle r^2\rangle$	[57–60]
	53, 55, 57, 59, 61, 63	Q_s	[61]
Ni, 28	58–68, 70	I, μ, Q_s, $\delta\langle r^2\rangle$	Under analysis.
Cu, 29	58–75, 68m, 70m1, 70m2	I, μ, Q_s, $\delta\langle r^2\rangle$	[47, 49, 62–64]
	63–66, 68–78, 68m, 70m1, 70m2	I, μ, Q_s, $\delta\langle r^2\rangle$	CRIS, under analysis.
Zn, 30	62–80, 69m–79m	I, μ, Q_s, $\delta\langle r^2\rangle$	[65] and under analysis.
Ga, 31	63, 64, 66–81, 80m	I, μ, Q_s	[50, 66, 67]
	63, 64, 66, 68–82, 80m	$\delta\langle r^2\rangle$	[68, 69]
	65, 67, 69, 71, 75, 79–82, 80m	I, μ, Q_s, $\delta\langle r^2\rangle$	CRIS, under analysis.
Cd, 48	100–129, 111m–129m	I, μ, Q_s, $\delta\langle r^2\rangle$	[70–72] and under analysis.
Sn, 50	109, 112–134	I, μ, Q_s, $\delta\langle r^2\rangle$	Under analysis.

Thus in the K isotopes, it is the increase of the attractive force between the $d_{3/2}$ protons and the neutrons filling the $f_{7/2}$ level that induces a stronger binding of the proton level, thus reducing the gap with the $\pi 1s_{1/2}$ level and even reversing these effective single-particle levels at $N = 28$. An open question was how this level inversion would change when the next neutron orbit, $p_{3/2}$ would be filled. That question was answered by hyperfine structure measurements on the K isotopes between $N = 18$ and 32. The ground state spin remains $1/2^+$ in ^{49}K but re-inverts back to $3/2^+$ in ^{51}K [51]. The composition of the ground state wave functions could be confirmed by the large scale shell model calculations which reproduced the measured magnetic moments very well [52].

In the Cu isotopes, it was predicted that in ^{75}Cu the $5/2^-$ level would become the ground state because of the increasing attraction between the $\pi 0f_{5/2}$ and the $\nu 0g_{9/2}$ orbits, leading to an inversion of the $p_{3/2}$ and $f_{5/2}$ proton effective single-particle levels at $N = 46$. High-resolution experiments on Cu isotopes using optical detection could be performed up to ^{75}Cu, establishing experimentally the spin inversion [49]. Low-resolution in-source resonance ionisation spectroscopy proposed a ground state spin/parity $5/2^-$ for ^{77}Cu as well [76], and this was recently confirmed by high-resolution studies up to ^{78}Cu, using the high-resolution CRIS technique (see section 3.3 for details on the method). Data are currently being analysed and details on spins, radii and moments will be extracted [77]. In the Ga isotopes ($Z = 31$) the inversion of the single-particle proton orbitals is not as clear-cut and a very rich ground state structure has been observed between $N = 40$ and $N = 50$ [50]. Up to ^{79}Ga the ground state spin is $3/2^-$, except for ^{73}Ga ($N = 42$) where the ground state was measured to be $1/2^-$, contrary to the earlier reported $3/2^-$. From the measured magnetic and quadrupole moments it could be inferred that the ground state wave functions gradually change from three protons in the $\pi p_{3/2}$ orbit for the stable ^{69,71}Ga to a very mixed wave function for the $1/2^-$ ground state in ^{73}Ga. The moments of ^{75,77}Ga are consistent with two protons in $\pi f_{5/2}$ and one proton in $\pi p_{3/2}$, while the full inversion of the proton $f_{5/2}$ and $p_{3/2}$ level occupations occurs in ^{79}Ga ($N = 48$) which has a leading $\pi {f_{5/2}}^3$ configuration, coupled to spin 3/2. Only at ^{81}Ga, at

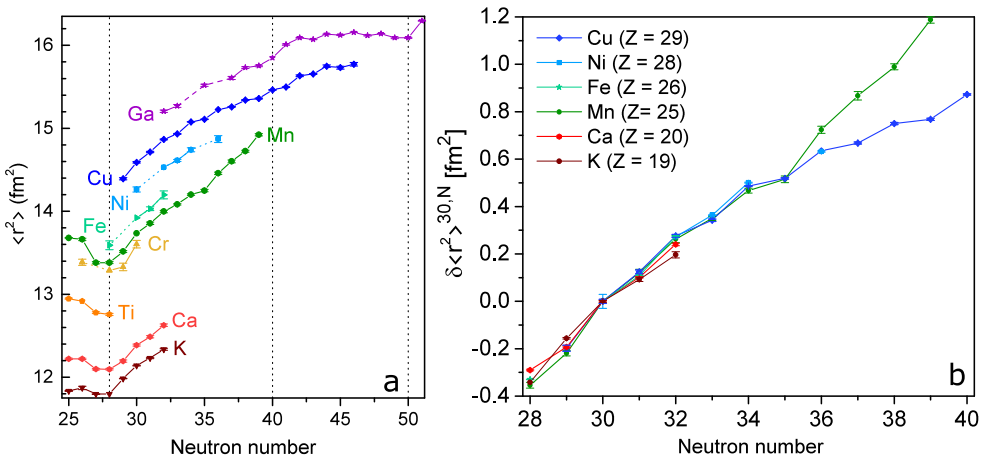

Figure 5. (a) Charge radii from K up to Ga from just below $N = 28$ up to $N = 40$. A decrease in the radii is seen towards $N = 28$ and a steep increase is observed when crossing the $N = 28$ shell gap. No signature for a shell closure at $N = 32$ is seen for Ca and K. Taken from [48, 54, 60, 64, 68]. (b) Radii relative to the $N = 30$ value for each isotopic chain: the radii follow a remarkable similar increase beyond $N = 28$, highlighting the sudden onset of deformation in the Mn radii beyond $N = 36$.

$N = 50$, does the ground state actually become $5/2^-$. Also, a new isomeric state was observed in ^{80}Ga [66] and its beta-decay properties were recently measured at ISOLDE [78]. Laser spectroscopy was also well-placed to confirm the existence of and firmly assign spins to long-lived isomeric states in the Zn isotopes. In particular an intruder isomeric state was established in ^{79m}Zn [65], which notably displayed a signature of shape coexistence.

3.2.2. Search for signatures of new magic numbers. *No evidence for an $N = 32$ shell gap.* A variety of spectroscopy experiments on neutron-rich isotopes with $Z \geqslant 20$ suggested the appearance of a new magic number at $N = 32$ towards ^{52}Ca [79–82]. Recent mass measurements up to ^{54}Ca confirmed that result and 'unambiguously establishes a prominent shell closure at neutron number $N = 32$' [83]. Furthermore, mass measurements up to ^{53}K confirmed the local 'doubly-magic' nature of ^{52}Ca [84].

However, in the mean square charge radii of the K isotopes, no clear evidence for a sub-shell closure at $N = 32$ is observed [54]. We also measured the mean square charge radii of the Ca isotopes from $N = 20$ up to 32, and also in these isotopes no signature of a shell effect at $N = 32$ is seen [48]. In figure 5(a), all recently measured (and published) charge radii from K up to Ga are shown. A clear increase is observed in the radii when crossing $N = 28$. For K and Ca, no flattening towards $N = 32$ is seen, which would be expected for a magic shell gap. Additionally, also from the magnetic moments of the odd-A Ca isotopes no signature for a shell closure at $N = 32$ is observed [55]. Indeed, the observed magnetic moment of ^{51}Ca, with 31 neutrons, requires excitations of neutrons across $N = 32$ in the higher pf-orbits, to reproduce the observed value. These results illustrate that more experimental studies on the single-particle nature of the ground state wave functions of Ca isotopes, such as transfer reaction experiments, are needed to further investigate this ambiguity.

Weak localised sub-shell effect at $N = 40$. In the neutron-rich Ni region, the presence of a magic number at $N = 40$ has been debated for several years in literature. By now it is commonly accepted that the signatures for the sub-shell gap (large $E(2^+)$ and low B(E2))

could also be induced by the fact that this is a gap between orbits with opposite parity, thus requiring at least two neutron excitations to mix into the normal wave function and thus leading to a more pure ^{68}Ni configuration (it has $E(2_1^+) > 2$ MeV). The magnetic and quadrupole moments of the Cu isotopes around ^{69}Cu suggest also a 'magic' behaviour for ^{69}Cu, but as for the excitation energies and transition probabilities this can also be understood as mostly due to the parity change [47, 63].

The nuclear charge radii could provide evidence of the existence of a shell gap at $N = 40$. A distinct upward kink in the course of charge radii as a function of neutron number is seen at all the major neutron-shell closures above $N = 20$ (i.e. 28, 50, 82, 126). We have measured the changes in nuclear mean square charge radii across the Cu [64] and Ga [68] isotope chains and the new data for Zn and Ni are under analysis. A cursory look at the Cu radii shows nothing remarkable but a close analysis [64], where the main volume-change contribution to radii is subtracted, does show a dip around $N = 40$ in both the odd-N and even-N systematics. A similar analysis of the Ga isotopes is less convincing, although there is a reversal of the normal odd–even staggering at $N = 40$ giving ^{71}Ga a smaller radius than the average trend would predict. The $E(2_1^+)$ systematics for Zn ($Z = 30$) isotopes, where the state is below 1 MeV in ^{70}Zn and actually lower than $E(2_1^+)$ in the lighter $^{60-68}$Zn isotopes, does not suggest to expect a signature in the radii for a $N = 40$ shell gap. It may only be evident in the Ni isotopes where the $Z = 28$ shell closure strengthens the doubly-magic effect.

3.2.3. Onset of deformation between Z = 20 and 28. In the region between $Z = 20$ and 28, the $\pi f_{7/2}$ orbital is gradually filled and an onset of deformation is expected around proton mid-shell. Therefore we have investigated the Mn ($Z = 25$) isotopes from $N = 26$ to 39. As the quadrupole moment is the most sensitive observable to static deformation, a hyperfine level with a sufficiently large electric field gradient has to be studied, which requires the population of a metastable state in the ion. This was achieved through optical pumping from the ionic ground state by laser excitation in ISCOOL [61]. We established firmly the ground state spin of all Mn isotopes and long-lived isomers up to ^{64}Mn [58, 59]. All odd-A Mn isotopes, except for ^{53}Mn at $N = 28$, have a ground state spin/parity $5/2^-$, that deviates from the expected $7/2^-$: this is a first signature for the non-spherical nature of these isotopes. A comparison of the magnetic and quadrupole moments with large scale shell model calculations in different model spaces shows that proton excitation across $Z = 28$ as well as neutron excitation across $N = 40$ and $N = 50$ (into the $g_{9/2}$ and $d_{5/2}$ orbits) are needed to reproduce the observed values from $N = 36$ onwards [58, 61]. The slope in the charge radii of the Mn isotopes clearly increases from $N = 36$ onwards, confirming the increase in deformation that was observed also in the quadrupole moments [60]. This is best seen in figure 5(b) where the charge radii of all isotopic chains are plotted relative to the value at $N = 30$. A remarkable similarity is seen in the trend of the radii beyond $N = 28$, contrary to e.g. the Pb region where the slope of the radii beyond $N = 126$ increases with proton number [85]. In the odd–odd $^{58-64}$Mn isotopes a long-lived isomeric state coexists with the ground state. We firmly established a spin 1 and a spin 4 to the two levels in each of these isotopes [59] and their magnetic moments are well reproduced by shell model calculations in the pf-space up to $N = 35$, while proton and neutron excitations outside this model spaces are needed from $N = 37$ onwards.

3.2.4. Simple structure in complex nuclei (Cd). Spectroscopy of cadmium at COLLAPS was originally motivated by nuclear astrophysics: the neutron-rich isotopes were expected to shed light on a shell-quenching hypothesis at $N = 82$ and its consequences for the duration of the

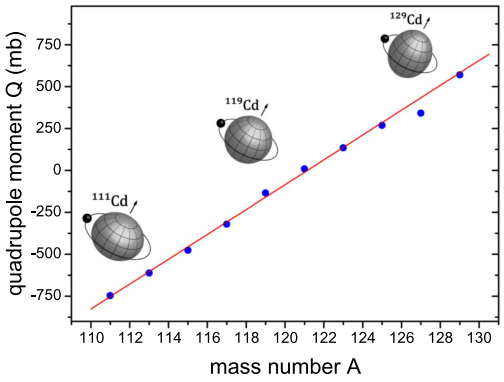

Figure 6. Quadrupole moments of $11/2^-$ isomeric states in the sequence of odd-A $^{111-129}$Cd. Shape changes with respect to the $h_{11/2}$ neutron movement are illustrated by inserted images.

r-process along the waiting-point nuclei below ^{130}Cd, whereas the neutron-deficient ones should elucidate the role of the cadmium isotopes in the rp-process for rapidly accreting neutron stars [86]. Surprisingly, the properties of the $11/2^-$ isomers in the range of $^{111-129}$Cd turned out to be of utmost interest since they are found to behave in an extremely predictable manner. While this can be partially understood in the conventional interpretation of the nuclear shell model, a full description must clearly go beyond this picture. Laser spectroscopy studies were performed on atomic Cd in the 5s5p $^3P_2 \rightarrow$ 5s6s $^3S_1$ transition as well as on Cd^+ in the 5s $^2S_{1/2} \rightarrow$ 5p $^2P_{3/2}$ transition. The latter required cw laser light at 214.5 nm, produced by fourth-harmonic generation of 860 nm light output of a titanium-sapphire laser.

Overall, the isotopes from ^{100}Cd up to the shell-closure at ^{130}Cd were studied and nuclear magnetic moments and electric quadrupole moments were extracted from the spectra using reference dipole moments and calculated electric field gradients, respectively. The electric quadrupole moments of the $11/2^-$ isomers extracted from the spectra are shown in figure 6 [70]. They exhibit an extremely linear behaviour along a chain of 10 isomers. According to the naive shell-model picture and assuming an effective charge for the (identical) neutrons filling the $h_{11/2}$ shell, a linear increase starting from an oblate nucleus, crossing zero at mid-shell and having maximum prolate deformation just before the shell-closure is expected. While this simple structure is at first sight reflected by the quadrupole moments, a second look reveals considerable differences from this model: the number of 10 odd-mass isomers is 4 more than the expected number for solely filling the $h_{11/2}$ shell and the zero-crossing is not exactly at mid-shell. In [70], a degeneracy of the $h_{11/2}$ and some of the neighbouring $s_{1/2}$, $d_{3/2}$, and $d_{5/2}$ orbitals has been suggested to explain these observations, giving rise to a kind of a 'super-shell' that is shared by the $I = 0$ neutron pairs. With this assumption, a single-particle quadrupole moment of $Q_{\mathrm{sp}} = -667(31)$ mbarn and a constant core deformation with $Q_{\mathrm{const}} = -85(8)$ mbarn can be extracted. This implies a rather large effective neutron charge of $q_{\mathrm{eff},n} = 2.5e$. Later it was shown that these assumptions can indeed be used to explain also the isomer shifts between the respective ground state and the isomer, which were found to follow a distinct parabolic dependence as a function of the atomic mass number [72]. Even though the nuclear shape is very close to spherical all along the isotopic chain and never exceeds a deformation parameter of 0.07, this unique regularity in the isomeric shift can be understood as a manifestation of nuclear deformation. Finally, the hyperfine structure anomaly for isotopes and isomers with $s_{1/2}$, $d_{5/2}$, and $h_{11/2}$ states was

evaluated and a linear relationship observed for all nuclear states except $s_{1/2}$. This is in accordance with the Moskowitz–Lombardi rule, being established in the mercury region of the nuclear chart, and was observed in all four atomic and ionic levels that were investigated [71].

3.3. Collinear resonance ionisation spectroscopy

The CRIS experiment at ISOLDE is based on a methodology first proposed by Kudriavtsev and Letokhov [87] and was previously demonstrated at ISOLDE with experiments that studied neutron-deficient ytterbium isotopes [88]. This initial work highlighted the method's low background and insensitivity to isobaric contamination with a signal-to-noise ratio of better than 20, while maintaining a spectroscopic linewidth of 50 MHz. The introduction of ion cooling and bunching methods for laser spectroscopy at the IGISOL facility [45] allowed the CRIS technique to be demonstrated on a bunched beam. In this way it was possible to improve the overall efficiency of the technique by several orders of magnitude by matching the ion trapping time with the duty cycle of the pulsed lasers used for ionisation [89, 90]. The installation of the gas-filled linear RFQ Paul trap (ISCOOL) [46] at ISOLDE, as part of the HIE-ISOLDE upgrade programme, stimulated the development of a new dedicated beam line with a UHV interaction region, for efficient bunched-beam CRIS.

The CRIS experiment is located in the low energy part of the ISOLDE hall [91, 92]. It uses the high-resolution mass separator (HRS) and the ISCOOL cooler-buncher. The trapping and release timing is synchronized to the pulsing cycle of a high-power laser, used for ionising a resonantly excited atom beam. After bunching, the ion beam is transported to a charge-exchange cell, which uses a potassium load heated to 170 °C to neutralise it into the atomic ground or metastable states. Any ions that are not neutralised are removed from the beam by an electrostatic deflector plate, positioned within a differential pumping region after the charge-exchange cell. The atom bunch then passes into a region of UHV (to avoid collisional re-ionisation) where it is collinearly overlapped with multiple laser beams, depending on the resonance ionisation scheme used. The 1.2 m length of the laser-atom interaction region is chosen to closely match the spatial dimensions of the ion bunches from ISCOOL. The resonantly produced ions are then deflected from the remaining atoms into a charged-particle detector (MCP) or transported to a decay spectroscopy station [93].

In order to allow a flexible choice of ionisation schemes, the CRIS experiment uses a variety of cw and pulsed laser systems. The two high-resolution cw lasers for scanning the high-resolution resonant excitation step have external-cavity frequency doubling units. They can be chopped [94] or pulse-amplified (either by a pulsed dye amplifier or injection seeded laser system). Additional steps within the resonance ionisation scheme are excited using either a pulsed dye laser or pulsed Z-cavity Ti:Sa laser. A 200 Hz Nd:YAG laser system is used for schemes which require a non-resonant ionisation step. Details on the lasers can be found in [95].

3.3.1. Francium measurements and results. The measurements on the francium isotope chain formed part of the commissioning phase of the CRIS experiment. This work was motivated by evidence for the phenomenon of shape coexistence in the neutron-deficient isotopes and isomers [96]. Towards the neutron-rich the aim was an extension of knowledge around the region of reflection asymmetry. Previously, measurements had been performed on $^{207-213}$Fr and $^{220-228}$Fr using laser spectroscopy on thermal atomic beams [97, 98]. To date the measurements cover 20 ground and isomeric states spanning the chain from ^{201}Fr to ^{233}Fr. The high selectivity and high resolution of the CRIS technique presented an opportunity to

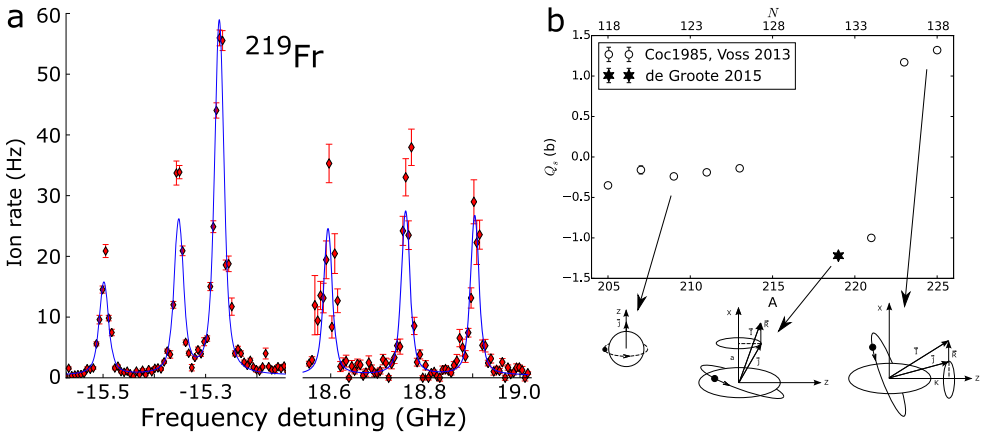

Figure 7. (a) Hyperfine structure spectrum of the 7s $^2S_{1/2} \rightarrow$ 8p $^2P_{3/2}$ transition in ^{219}Fr. A resolution of 20 MHz was achieved by separating the resonant excitation laser light from the non-resonant ionisation laser light in time [94]. (b) In the quadrupole moments of odd-*A* francium ground states (from [94, 97, 107]) strong changes of nuclear deformation are observed, from quasi-spherical below $N = 126$ to strong oblate or prolate deformation around mass 222.

separate low energy nuclear isomers and subsequently perform nuclear decay spectroscopy in quasi-background-free conditions.

The initial experiments used a frequency-doubled pulsed Ti:Sa laser from RILIS [99] to produce the 422 nm light with a linewidth of 1.5 GHz to excite the 7s $^2S_{1/2} \rightarrow$ 8p $^2P_{3/2}$ transition. This laser can scan across more than 100 GHz, which is essential for francium which has hyperfine structures that exceed 60 GHz. These experiments measured the isotope shift and magnetic moments of $^{202-206}$Fr, with a total experimental efficiency of 1% [100, 101], allowing the study of isotopes with yields as low a 100 ions s^{-1}. This work observed a small departure in the $\delta\langle r^2\rangle$ from the lead and polonium trend [102, 103] at ^{202,203}Fr but found no evidence in the measured *g*-factors for an onset of static deformation [101]. A UHV compatible alpha-decay spectroscopy station [93] was used to study ^{204}Fr, allowing unambiguous identification of the two isomeric states and also to identify overlapping hyperfine components [101]. Beyond $N = 126$, hyperfine spectra and isotope shifts were measured for ^{218m,219,229,231}Fr. The $\delta\langle r^2\rangle$ and associated trend in odd–even staggering was found to be consistent with a deformed configuration for ^{218m,219}Fr and ^{220}Fr marks the border of the region of reflection asymmetry [104]. The *g*-factor of ^{219}Fr further supported this interpretation as it closely matched those of ^{221,223,225}Fr, which are known to be well-deformed nuclei [104]. The 1.5 GHz linewidth laser system has proved an ideal method for rapidly locating resonances, which has been recently demonstrated by the measurement of the hyperfine structure and isotope shift of ^{214}Fr. With a half-life of 5(1) ms, this is the shortest-lived nuclear ground state to be measured with laser spectroscopy [85, 105], where ISOL production is the limiting factor.

A much higher resolution is required to fully resolve each hyperfine component from which spectroscopic quadrupole moments and spin assignments can be deduced. This was achieved by chopping cw laser light into 100 ns long pulses using a Pockels cell, and then delaying the 1064 nm light from a high power Nd:YAG laser until the cw light had just been extinguished. This method eliminated effects associated with the strong light field and allowed a linewidth of 20(1) MHz to be achieved, while saturating both transitions [94, 106].

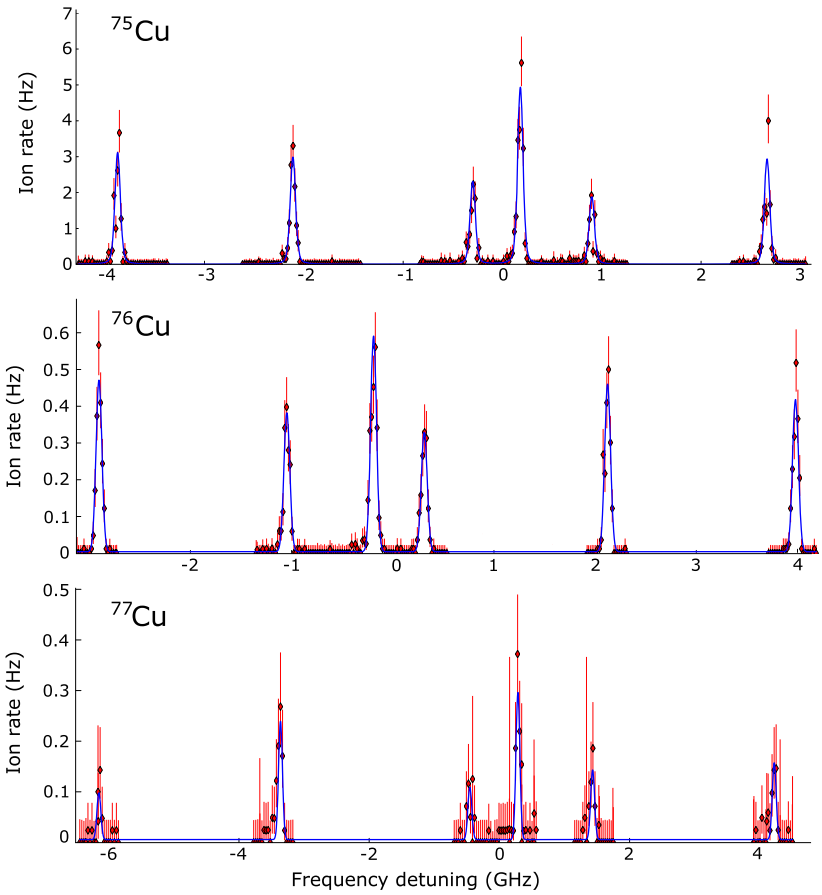

Figure 8. Hyperfine structure spectra of ^{75}Cu, ^{76}Cu and ^{77}Cu using high-resolution resonance ionisation spectroscopy in the $^{2}S_{1/2}$ to $^{4}P_{3/2}$ transition at 249 nm.

With this method the spectroscopic quadrupole moment of ^{219}Fr could be determined from the observed hyperfine structure shown in figure 7(a). The quadrupole moment confirmed that the structure of ^{219}Fr is quite different from the shell-model description of a nucleus with a half-filled $\pi h_{9/2}$ orbital, where an almost zero quadrupole moment is expected (and observed for $A < 215$) (figure 7(b)). The measured quadrupole moment confirms a static deformed shape, and its negative value results from Coriolis mixing of the prolate structure that leads to a decoupling of the odd-particle spin from the deformation axis ($K < I$). The rapid change in sign of the ground state quadrupole moments in the odd-A isotopes $^{219-225}$Fr is consistent with the change in bands from $K = 1/2^{-}$ in ^{219,221}Fr to $K = 3/2^{-}$ in ^{223,225}Fr, and the associated change in coupling strength to the deformation axis.

The combination of high-resolution CRIS and α-decay spectroscopy was able to unambiguously assign all hyperfine structure components for the ground and two isomeric states in ^{206}Fr [108]. The branching ratios of the isomeric states could be studied in complete isolation from one another for the first time. Thus the hindrance factors could be determined for each decay chain, allowing a firm assignment of the spins and configurations of the states in ^{202}At and ^{198}Bi.

3.3.2. Towards CRIS in intermediate and low mass regions. In the last two years, high-resolution CRIS measurements have been performed successfully on the Ga and Cu isotopes, extending our earlier studies towards more neutron-rich isotopes. The data are being analysed and example spectra for ^{75,77}Cu are shown in figure 8. For copper the sensitivity of the CRIS method has been pushed now to a few 10 ions s^{-1}, allowing the study of ^{78}Cu. Further improvements should be possible in ionisation efficiency as well as background reduction, giving hope for a study of ^{79}Cu with less than 10 ions s^{-1}.

4. Future directions

The determination of nuclear ground state properties along isotopic chains from collinear laser spectroscopy is now indispensable in nuclear physics research with radioactive beams. Many sub-disciplines of nuclear physics, like the evolution of nuclear structure with neutron excess, nuclear astrophysics, and tests of fundamental symmetries have profited a lot from the unrivalled precision and sensitivity that has been demonstrated by high-resolution laser spectroscopy, as laid out above.

The success of this method can best be seen by the fact that almost all radioactive beam facilities in the world have meanwhile an active or planned programme for laser spectroscopy, including all future facilities. Despite the tremendous progress made in this field over the past decades, large unexplored regions still remain in the nuclear chart that have not yet been investigated with laser spectroscopy partly because of a lack of accessible transitions/wavelengths or a lack of yield and there is always the quest for higher sensitivity and efficiency in order to reach more and more exotic species which are produced in less and less quantities. Presently there are three main paths followed as future directions in precision laser spectroscopy in nuclear physics research, two of them based on stored charged particles:

- Recently an electrostatic ion beam trap (EIBT) for ultra-sensitive collinear laser spectroscopy of radionuclides was proposed by Stephan Ettenauer at ISOLDE and funded by an ERC starting grant. The idea is to employ an EIBT, also called multi-reflection time-of-flight system [109], in order to overcome the sensitivity limit of conventional collinear laser spectroscopy, where currently about 10^3 ions per second are needed to get useful spectra. In an EIBT the ions of interest are confined by reflecting them in-between two electrostatic mirrors separated by about 0.5 m [110] with a revolution frequency of typically a few kHz. In this way the laser-ion interaction time can be dramatically increased and thus the sensitivity of collinear laser spectroscopy. The minimum required number of ions per second to perform a successful measurement of nuclear properties like charge radii and moments can be reduced to one or a few depending on the half-life and the transition scheme of the ion of interest. At beam energies of a few ten keV within the EIBT Doppler broadening of the natural line width can still be reduced similarly as in conventional collinear laser spectroscopy.
  This novel approach is particularly well suited for closed two-level systems in which laser-excited ions decay back into their initial state. In the general case, optical pumping into other hyperfine or metastable fine structure states has to be considered. Techniques to re-establish the initial state distribution, e.g. by repump transitions using additional lasers, will be explored experimentally within the ERC project, to fully take advantage of an EIBT in terms of its enhanced sensitivity for collinear laser spectroscopy.
- The heavy ion storage ring TSR supported for more than 20 years at the Max-Planck-Institut für Kernphysik in Heidelberg a strong research programme in the fields of atomic, molecular and accelerator physics. In 2012 it was proposed to move this ring with a

circumference of 55 m to ISOLDE and to install it behind the post-accelerator with injection energies up to 10 MeV A^{-1} [111]. The TSR provides excellent opportunities to study challenging cases which could not be addressed at ISOLDE so far. Among others, at energies of about 10 Mev A^{-1} the rest frame wavelengths will be Doppler shifted by up to 30 nm, thus providing access to the ultraviolet wavelength region, which is otherwise due to a lack of lasers difficult to probe. Furthermore, due to the possibility to accumulate and recirculate (up to 10^5 times per second) an ion beam in a storage ring, a significant gain in experimental efficiency and sensitivity can be obtained, since the same ion can be probed many times provided that the level scheme allows for it. In order to reduce the Doppler width due to the longitudinal momentum spread of the heavy ion beam, electron cooling is applied which yields about $\delta p/p = 6 \times 10^{-5}$ resulting in a typical line width of $\delta\nu \approx 2$ GHz. For highly charged ions this is sufficient since hyperfine splittings are typically one to two orders of magnitude greater than this. Still, due to the long electron cooling time of a few seconds this technique can only be applied to a few specific cases.

A most compelling case for spectroscopy in TSR will be the He-like ionic systems up to oxygen. For those systems the $^3S_1 - {}^3P_0$ transition can be calculated exactly, allowing absolute charge radii to be measured from transition frequencies. The limitation to $Z \leqslant 8$ is given by the laser wavelength which for oxygen can be shifted to 189.5 nm for exiting the transition at the rest-frame wavelength of 164.0 nm. Such absolute charge radii measurements taking advantage of the TSR would be feasible for boron, carbon, nitrogen and oxygen.

Presently the TSR at ISOLDE project is put on hold by the CERN management due to too high installation costs, but the possibility of performing laser spectroscopy on exotic species in a storage ring is still of high interest.

- A third line of developments are particle-sensitive techniques in combination with collinear laser spectroscopy as they have been used previously since they are extremely sensitive. Examples are state-selective charge exchange [112], which provides access to very exotic isotopes of alkaline earth elements or state-selective collisional ionisation which has been used for rare gases and has now been proposed as well for fluorine.

Acknowledgments

We gratefully acknowledge support by the German Ministry for Education and Research (BMBF) and the Max-Planck-Society, the Belgian Flemish Science Foundation (FWO), the KU Leuven Research Council and the Interuniversity Attraction Poles program, and the UK Science and Technology Facilities Council. Travel support (subsistence) was provided by the European Union seventh framework through ENSAR. We also wish to thank the ISOLDE technical group for their continuous commitment to our projects.

References

[1] Kopfermann H 1958 *Nuclear Moments* (New York: Academic)
[2] Neugart R 1981 *Nucl. Instrum. Methods Phys. Res.* **186** 165
[3] Mueller A C *et al* 1983 *Nucl. Phys.* A **403** 234
[4] Geithner W *et al* 2000 *Hyperfine Interact.* **127** 117
[5] Marinova K *et al* 2011 *Phys. Rev.* C **84** 034313
[6] Klein A *et al* 1996 *Nucl. Phys.* A **607** 1

[7] Lievens P *et al* 1991 *Phys. Lett.* B **256** 141
[8] Vermeeren L *et al* 1992 *Phys. Rev. Lett.* **68** 1679
[9] Geithner W *et al* 1999 *Phys. Rev. Lett.* **83** 3792
[10] Keim M *et al* 2000 *Eur. Phys. J.* A **8** 31
[11] Neugart R *et al* 2008 *Phys. Rev. Lett.* **101** 132502
[12] Kowalska M *et al* 2008 *Phys. Rev.* C **77** 034307
[13] Frånberg H *et al* 2008 *Nucl. Instrum. Methods Phys. Res.* B **266** 4502
[14] Marsh B *et al* 2013 *Nucl. Instrum. Methods Phys. Res.* B **317** 550
[15] Seliverstov M D *et al* 2013 *Phys. Lett.* B **719** 362
[16] Fricke G and Heilig K 2004 Nuclear charge radii *Springer Materials—The Landolt–Börnstein Database* ed H Schopper vol 20 (Berlin: Springer)
[17] Kaufman S 1976 *Opt. Commun.* **17** 309
[18] Campbell P, Moore I and Pearson M 2016 *Prog. Part. Nucl. Phys.* **86** 127
[19] Blaum K, Dilling J and Nörtershäuser W 2013 *Phys. Scr.* **T152** 014017
[20] Cheal B and Flanagan K T 2010 *J. Phys. G: Nucl. Part. Phys.* **37** 113101
[21] Arnold E *et al* 1987 *Phys. Lett.* B **197** 311
[22] Tanihata I *et al* 1985 *Phys. Rev. Lett.* **55** 2676
[23] Arnold E *et al* 1992 *Phys. Lett.* B **281** 16
[24] Borremans D *et al* 2005 *Phys. Rev.* C **72** 044309
[25] Sánchez R *et al* 2006 *Phys. Rev. Lett.* **96** 033002
[26] Nörtershäuser W, Neff T, Sánchez R and Sick I 2011 *Phys. Rev.* C **84** 024307
[27] Navrátil P and Barrett B R 1998 *Phys. Rev.* C **57** 3119
[28] Motobayashi T *et al* 1995 *Phys. Lett.* B **346** 9
[29] Neyens G *et al* 2005 *Phys. Rev. Lett.* **94** 022501
[30] Maréchal F *et al* 2005 *Phys. Rev.* C **72** 044314
[31] Yordanov D T *et al* 2007 *Phys. Rev. Lett.* **99** 212501
[32] Yordanov D T *et al* 2010 *Phys. Rev. Lett.* **104** 129201
[33] Yordanov D T *et al* 2012 *Phys. Rev. Lett.* **108** 042504
[34] Krieger A *et al* 2011 *Nucl. Instrum. Methods Phys.* A **632** 23
[35] Krieger A *et al* 2017 *Appl. Phys.* B **123** 15
[36] Yan Z C and Drake G W F 2000 *Phys. Rev.* A **61** 022504
[37] Puchalski M and Pachucki K 2008 *Phys. Rev.* A **78** 052511
[38] Yan Z C, Nörtershäuser W and Drake G W F 2008 *Phys. Rev. Lett.* **100** 243002
[39] Jansen J, Peerdeman R and Vries C D 1972 *Nucl. Phys.* A **188** 337
[40] Nörtershäuser W *et al* 2009 *Phys. Rev. Lett.* **102** 062503
[41] Žáková M *et al* 2010 *J. Phys. G: Nucl. Part. Phys.* **37** 055107
[42] Krieger A *et al* 2012 *Phys. Rev. Lett.* **108** 142501
[43] Nörtershäuser W *et al* 2015 *Phys. Rev. Lett.* **115** 033002
[44] Puchalski M and Pachucki K 2014 *Phys. Rev. Lett.* **113** 073004
[45] Nieminen A *et al* 2002 *Phys. Rev. Lett.* **88** 094801
[46] Mané E *et al* 2009 *Eur. Phys. J.* A **42** 503
[47] Vingerhoets P *et al* 2010 *Phys. Rev.* C **82** 064311
[48] Garcia Ruiz R *et al* 2016 *Nat. Phys.* **12** 594
[49] Flanagan K T *et al* 2009 *Phys. Rev. Lett.* **103** 142501
[50] Cheal B *et al* 2010 *Phys. Rev. Lett.* **104** 252502
[51] Papuga J *et al* 2013 *Phys. Rev. Lett.* **110** 172503
[52] Papuga J *et al* 2014 *Phys. Rev.* C **90** 034321
[53] Bissell M L *et al* 2014 *Phys. Rev. Lett.* **113** 052502
[54] Kreim K *et al* 2014 *Phys. Lett.* B **731** 97
[55] Garcia Ruiz R F *et al* 2015 *Phys. Rev.* C **91** 041304
[56] Garcia Ruiz R F 2015 *PhD Thesis* KU Leuven, Belgium
[57] Heylen H *et al* 2015 *Acta Phys. Pol.* B **46** 699
[58] Babcock C *et al* 2015 *Phys. Lett.* B **750** 176
[59] Heylen H *et al* 2015 *Phys. Rev.* C **92** 044311
[60] Heylen H *et al* 2016 *Phys. Rev.* C **94** 054321
[61] Babcock C *et al* 2016 *Phys. Lett.* B **760** 387
[62] Flanagan K T *et al* 2010 *Phys. Rev.* C **82** 041302
[63] Vingerhoets P *et al* 2011 *Phys. Lett.* B **703** 34

[64] Bissell M L *et al* 2016 *Phys. Rev.* C **93** 064318
[65] Yang X F *et al* 2016 *Phys. Rev. Lett.* **116** 182502
[66] Cheal B *et al* 2010 *Phys. Rev.* C **82** 051302
[67] Mané E *et al* 2011 *Phys. Rev.* C **84** 024303
[68] Procter T J *et al* 2012 *Phys. Rev.* C **86** 034329
[69] Cheal B *et al* 2012 *J. Phys.: Conf. Ser.* **381** 012071
[70] Yordanov D T *et al* 2013 *Phys. Rev. Lett.* **110** 192501
[71] Frömmgen N *et al* 2015 *Eur. Phys. J.* D **69** 164
[72] Yordanov D T *et al* 2016 *Phys. Rev. Lett.* **116** 032501
[73] Touchard F *et al* 1982 *Phys. Lett.* B **108** 169
[74] Franchoo S *et al* 1998 *Phys. Rev. Lett.* **81** 3100
[75] Otsuka T *et al* 2005 *Phys. Rev. Lett.* **95** 232502
[76] Köster U *et al* 2011 *Phys. Rev.* C **84** 034320
[77] de Groote R P *et al* 2017 in preparation
[78] Lica R *et al* 2014 *Phys. Rev.* C **90** 014320
[79] Huck A *et al* 1985 *Phys. Rev.* C **31** 2226
[80] Janssens R *et al* 2002 *Phys. Lett.* B **546** 55
[81] Fornal B *et al* 2004 *Phys. Rev.* C **70** 064304
[82] Gade A *et al* 2006 *Phys. Rev.* C **74** 021302
[83] Wienholtz F *et al* 2013 *Nature* **498** 346
[84] Rosenbusch M *et al* 2015 *Phys. Rev. Lett.* **114** 202501
[85] Farooq-Smith G J *et al* 2016 *Phys. Rev.* C **94** 054305
[86] Atanasov D *et al* 2015 *Phys. Rev. Lett.* **115** 232501
[87] Kudriavtsev Y A and Letokhov V S 1982 *Appl. Phys.* B **29** 219
[88] Schulz C *et al* 1991 *J. Phys. B: At. Mol. Opt. Phys.* **24** 4831
[89] Flanagan K T 2004 *PhD Thesis* University of Manchester, UK
[90] Campbell P *et al* 2002 *Eur. Phys. J.* A **15** 45
[91] Procter T J *et al* 2012 *J. Phys.: Conf. Ser.* **381** 012070
[92] Cocolios T *et al* 2013 *Nucl. Instrum. Methods Phys. Res.* B **317** 565
[93] Rajabali M *et al* 2013 *Nucl. Instrum. Methods Phys. Res.* A **707** 35
[94] de Groote R P *et al* 2015 *Phys. Rev. Lett.* **115** 132501
[95] de Groote R P, Lynch K M and Wilkins S G 2017 *Hyperfine Interact.* **238** 5
[96] Uusitalo J *et al* 2005 *Phys. Rev.* C **71** 024306
[97] Coc A *et al* 1985 *Phys. Lett.* B **163** 66
[98] Coc A *et al* 1987 *Nucl. Phys.* A **468** 1
[99] Rothe S *et al* 2013 *Nucl. Instrum. Methods Phys. Res.* B **317** 561
[100] Flanagan K T *et al* 2013 *Phys. Rev. Lett.* **111** 212501
[101] Lynch K M *et al* 2014 *Phys. Rev.* X **4** 011055
[102] Witte H D *et al* 2007 *Phys. Rev. Lett.* **98** 112502
[103] Seliverstov M *et al* 2013 *Phys. Lett.* B **719** 362
[104] Budinčević I *et al* 2014 *Phys. Rev.* C **90** 014317
[105] Cocolios T *et al* 2016 *Nucl. Instrum. Methods Phys.* B **376** 284
[106] de Groote R P 2017 *Phys. Rev.* A **95** 032502
[107] Voss A *et al* 2013 *Phys. Rev. Lett.* **111** 122501
[108] Lynch K M *et al* 2016 *Phys. Rev.* C **93** 014319
[109] Wollnik H and Przewloka M 1990 *Int. J. Mass Spectrom.* **96** 267
[110] Wolf R *et al* 2012 *Nucl. Instrum. Methods Phys. Res.* A **686** 82
[111] Grieser M *et al* 2012 *Eur. Phys. J. Spec. Top.* **207** 1
[112] Garcia Ruiz R F *et al* 2017 *J. Phys. G: Nucl. Part. Phys.* accepted